An analysis of nuclear parton distribution function based on relative entropy*

Shu-Man Hu (胡书曼)† Ao-Sheng Xiong (熊傲昇)‡ Ji Xu (徐吉)§
Fu-Sheng Yu (于福升)♮ Ji-Xin Yu (余纪新)♯

Frontiers Science Center for Rare Isotopes, and School of Nuclear Science and Technology, Lanzhou University, Lanzhou 730000, China

Abstract: In this work, we propose a method for quantifying the difference between nuclear parton distribution functions in different nuclei and parton distribution functions in free nucleons using relative entropy (also known as the Kullback-Leibler divergence), a measure widely employed in quantum information theory. By introducing certain constraints and the "minimum relative entropy" hypothesis, we can determine the shape of the structure function in the intermediate-x region, which is closely connected to the renowned EMC effect. For quark structure functions, our results are consistent with the latest global fits to experimental data. This agreement suggests that the relative entropy-based methodology may provide novel insights into nucleon structure, particularly in cases where experimental data and theoretical QCD constraints are limited, such as those relevant to gluon nPDFs. Therefore, we apply this methodology to gluon nPDFs, analyzing the results from two commonly used global fitting groups, EPPS21 and nNNPDF3.0. Our analysis suggests that the central values of EPPS21 align more closely with the "minimum relative entropy" hypothesis. This finding underscores the utility of the proposed method and provides a valuable reference for future global fits of nPDFs.

Keywords: EMC effect, parton distribution function, nuclear parton distribution function

DOI: 10.1088/1674-1137/ae6da1 **CSTR:**

I. INTRODUCTION

Parton distribution functions (PDFs) are quantum correlation functions that characterize the probability that a parton carries a certain momentum fraction of the hadron momentum. PDFs serve as fundamental inputs for precision Standard Model (SM) baseline predictions at the LHC and other collider facilities, and thus their determination is a key focus in high-energy physics [1−6].

When free nucleons become bound within atomic nuclei, nuclear parton distribution functions (nPDFs) become necessary. One of the primary goals of nuclear physics is to achieve a comprehensive description of the structure of atomic nuclei. The nPDFs, which describe the motion of partons in the nuclear medium, remain one of the least understood aspects of nuclear structure. A prime example is the unexpected EMC effect, which indicates that quark PDFs in bound nucleons are modified compared with those in free nucleons in the intermediate-x region [7−10]. The complex nature of nonperturbative QCD renders an analytical solution for nPDFs unattainable. Furthermore, lattice QCD also remains impractical for this issue, as nuclear structure represents a quintessential many-body problem that currently exceeds the computational capabilities and resources available for lattice simulations. Even for very light nuclei, current lattice calculations remain at an exploratory stage [11−13]. Therefore, nearly all currently available nPDFs are extracted from global-fit analyses of experimental data [14−17].

Moreover, our knowledge of gluon nPDFs is consid-

Received 12 March 2026; Accepted 13 May 2026

* This work is supported in part by the National Natural Science Foundation of China under Grant No. 12335003, the Fundamental Research Funds for the Central Universities under Nos. lzujbky-2023-stlt01, lzujbky-2024-oy02, and lzujbky-2025-eyt01, and the Scientific Research Innovation Capability Support Project for Young Faculty under Grant No. ZYGXQNJSKYCXNLZCXM-P2. J.X. is supported in part by the National Natural Science Foundation of China under Grant Nos. 12475098 and 12105247

† E-mail: hushm2025@lzu.edu.cn
‡ E-mail: Corresponding author. xiongash21@lzu.edu.cn
§ E-mail: Corresponding author. xuji@lzu.edu.cn
♮ E-mail: Corresponding author. yufsh@lzu.edu.cn
♯ E-mail: Corresponding author. yujx18@lzu.edu.cn

erably more limited. While modern global-fit analyses yield increasingly precise quark nPDFs —with nuclear modifications for quarks in the intermediate-to-large x region being broadly consistent across different fitting groups—the gluon nPDF remains substantially more uncertain. In contrast to the quark sector, predictions for gluons from different groups often differ markedly. Therefore, developing new methodologies to constrain parton, especially gluon, nPDFs is a significant scientific goal.

The recent rapid development of quantum information theory has drawn attention in high-energy physics because of its potential applications to long-standing problems and its ability to reveal fundamental connections to underlying physical mechanisms [18, 19]. Quantum information theory has introduced novel observables—various types of entropies that enable an extended characterization of hadron structure and scattering processes beyond classical approaches. Studies in this area have proliferated significantly [20−37]. Here, we seek to identify an appropriate entropy for the investigation of nPDFs. First, both PDFs and nPDFs are probability distributions. Second, we aim to quantify the difference between these two distributions. The appropriate quantity is the Kullback-Leibler (KL) divergence $\int p(x)\ln(p(x)/q(x))dx$ (also known as relative entropy) [38−42], which is a type of statistical distance: a measure of how much a true distribution $p(x)$ differs from a reference distribution $q(x)$. If we treat the PDF as the reference distribution and the nPDF as the true distribution, their ratio reflects the nuclear modification, whose fundamental mechanism may be recast in the quantum-theoretic terms of KL divergence. When a free nucleon is placed inside an atomic nucleus, its PDFs are modified into nPDFs due to interactions with surrounding nucleons. Understanding the precise mechanism of this transformation remains a challenge. This paper explores an information-theoretic approach to this problem, elaborating on how concepts such as the "minimum relative entropy" hypothesis can shed new light on this transformation.

In this paper, we quantify the difference between PDFs and nPDFs using KL divergence. In the quark sector, we determine the nuclear structure function in the intermediate-x (EMC) region, where it is primarily sensitive to the underlying quark nuclear modifications, by invoking the minimum relative entropy hypothesis. This hypothesis proposes that when a free nucleon is bound in a nucleus, its PDFs transform into nPDFs in a way that minimizes the relative entropy between them, subject to known physical constraints. This approach frames the transformation as an optimization problem with fixed boundary conditions, providing a principle for determining the shape of nPDFs. In turn, this methodology offers a potential reference for assessing the quality of global fits to gluon nPDFs, which will be elaborated below.

The organization of this paper is as follows. In Sec. II, we give the formalism for structure functions in deeply inelastic scattering (DIS). Sec. III presents the definition of KL divergence and discusses its properties. In Sec. IV, we develop a framework and present results for quantifying and determining quark structure functions using the KL divergence. We turn to the investigation of gluon nPDFs in Sec. V. We finish with the conclusion in Sec. VI.

II. FORMALISM FOR STRUCTURE FUNCTIONS IN DIS

The cross sections for neutral-current DIS ($eN \to eX$) on unpolarized nucleons can be expressed in terms of structure functions

$$\frac{d^2\sigma_{\rm DIS}}{dxdy} = \frac{4\pi\alpha^2}{Q^4} s\Big((1-y)F_2(x,Q^2) + y^2 xF_1(x,Q^2)\Big), \tag{1}$$

where x is the Bjorken scaling variable, y denotes the inelasticity, Q^2 represents the negative of the squared four-momentum transfer from the lepton to the hadron, and s stands for the squared center-of-mass energy. It should be noted that Eq. (1) includes only the neutral-current photon-exchange contribution at leading order (LO) in the strong coupling constant α_s, and this equation can be further reduced using the Callan–Gross relation, $F_2 = 2xF_1$ [43].

$$\frac{d^2\sigma_{\rm DIS}}{dxdy} = \frac{2\pi\alpha^2}{Q^4} s\Big(1+(1-y)^2\Big)F_2(x,Q^2). \tag{2}$$

The simplified form in Eq. (2) is adopted in this study to facilitate the subsequent analysis based on the KL divergence. At LO, the relationship between the structure function F_2 and the quark distributions is given by

$$F_2(x,Q^2) = \sum_q e_q^2 x\Big[f_q(x,Q^2) + f_{\bar{q}}(x,Q^2)\Big], \tag{3}$$

where e_q denotes the electric charge of quark q, and $f_q(\bar{f_q})$ represents the PDF of parton (antiparton) q. In the case of an atomic nucleus, the structure function becomes

$$F_2^A(x,Q^2)/A = \sum_q e_q^2 x\Big[\frac{Z}{A}\Big(f_q^{p/A}(x,Q^2) + f_{\bar{q}}^{p/A}(x,Q^2)\Big) + \frac{N}{A}\Big(f_q^{n/A}(x,Q^2) + f_{\bar{q}}^{n/A}(x,Q^2)\Big)\Big], \tag{4}$$

where Z is the atomic number, N is the neutron number, and A is the mass number of the nucleus. $f_q^{p/A}$ denotes the nPDF of parton q in a proton bound in a nucleus with mass number A, and $f_q^{n/A}$ denotes the corresponding nP-

DF in a bound neutron.

For concision, we adopt the following notation:

$$\begin{cases} f_q^A(x,Q^2) = \dfrac{Z}{A} f_q^{p/A}(x,Q^2) + \dfrac{N}{A} f_q^{n/A}(x,Q^2), \\ f_{\bar{q}}^A(x,Q^2) = \dfrac{Z}{A} f_{\bar{q}}^{p/A}(x,Q^2) + \dfrac{N}{A} f_{\bar{q}}^{n/A}(x,Q^2). \end{cases} \tag{5}$$

Therefore, the structure function of nucleus A can be simplified as follows:

$$F_2^A(x,Q^2)/A = \sum_q e_q^2 x\left[f_q^A(x,Q^2) + f_{\bar{q}}^A(x,Q^2)\right]. \tag{6}$$

Numerous experimental and theoretical studies have been dedicated to describing this structure function [44−52]. Although substantial information about it is available, the exact distributions still cannot be obtained from first principles. The best currently available results come from global fits to experimental data. For instance, the EPPS21 Collaboration provides numerical values for f_q^A and $f_{\bar{q}}^A$ [53], which show good agreement with experimental results [54−58].

The EMC effect describes the deviation from unity in the ratio of per-nucleon deep inelastic structure functions for nucleus A to deuteron, $(F_2^A(x,Q^2)/A)/(F_2^d(x,Q^2)/2)$, in the intermediate-$x$ region. This deviation may, in turn, leave a signature on quantum information-theoretic quantities such as the KL divergence and serve as a proxy for nuclear modifications to the nucleon structure.

III. THE KULLBACK-LEIBLER DIVERGENCE

In this work, we use the KL divergence between PDFs and nPDFs to assess nuclear modifications. To make the discussion self-contained, we begin with a brief introduction to the KL divergence. Mathematically, the KL divergence between two probability distributions is defined as

$$D_{\mathrm{KL}}(p\|q) = \int p(x)\ln\frac{p(x)}{q(x)}dx. \tag{7}$$

From here on, we will denote $q(x)$ as the reference distribution and $p(x)$ as the true distribution. Here, we employ the KL divergence, which is also referred to as relative entropy in the literature, with units of *nats* (with the base of the logarithm e).

KL divergence is a fundamental quantity in probability and quantum information theory. It arises as the expected logarithm of the likelihood ratio of two distributions, $p(x)$ and $q(x)$. In what follows, we outline its distinguishing features. The KL divergence is a measure of the "distance" between the reference probability function $q(x)$ and the true probability function $p(x)$. It is always a non-negative real number, with value 0 if and only if the true function is identical to the reference function. The nonnegativity of the KL divergence implicitly assumes a prerequisite condition: both functions $q(x)$ and $p(x)$ are normalized to unity, $\int q(x)dx = 1$, $\int p(x)dx = 1$.

As discussed above, the KL divergence is a useful tool for quantifying the difference between nuclear and free-nucleon distributions. In the quark sector, our analysis is formulated at the level of structure functions that are linear combinations of quark and antiquark nPDFs. In the gluon sector, the same idea is applied directly to the gluon nPDFs. We now turn to these two applications in the following sections.

IV. FRAMEWORK AND RESULTS FOR QUARK STRUCTURE FUNCTIONS

In this section, we provide a method for calculating the KL divergence for different nuclei. The EMC experiment measured the ratio of per-nucleon structure functions between a nucleus A and the deuteron, $(F_2^A(x,Q^2)/A)/(F_2^d(x,Q^2)/2)$, which is closely related to the nuclear modification of quark nPDFs. Therefore, determining the shape of this ratio in the EMC region provides important constraints on the corresponding quark distributions. Theoretically, a major advantage of employing this ratio is its insensitivity to higher-order perturbative QCD corrections, as such perturbative contributions largely cancel in the ratio and are less relevant to the nonperturbative PDFs and nPDFs. Here, we take the numerator of this ratio as the true distribution $p^A(x)$ and the denominator as the reference distribution $q^d(x)$. In this work, $Q^2 = 10\,\mathrm{GeV}^2$, which is a typical scale in DIS processes. To keep the notation concise, the explicit Q^2 dependence is omitted.

For the reference distribution, the deuteron is regarded as an approximation to a free proton-neutron system because it is loosely bound and the average distance between the nucleons is large. Therefore, we adopt the CT18A free PDFs to construct the deuteron reference structure function [1]. For the true distribution, we use values from the EPPS21 parametrization for different nuclei[1)] [14]. First, we evaluate the KL divergence over the full-x interval. Because this interval includes the shadowing, antishadowing, EMC, and Fermi-motion regions, it provides a useful overall comparison of the nuclear and deuteron structure functions and serves as supplementary background for the subsequent analysis in the EMC region. Since we perform the numerical integration using global-fit results, we cannot directly compute the KL divergence over the idealized full range $x \in [0,1]$. Here, the

1) https://research.hip.fi/qcdtheory/nuclear-pdfs/epps21/

range for numerical integration is $x \in [10^{-6}, 0.99]$, which gives rise to a technical issue related to normalization. As introduced previously, the nonnegativity of the KL divergence inherently requires that both distributions be individually normalized to unity. Otherwise, the calculated KL divergence could yield negative values, which is counterintuitive for a measure representing any form of entropy. Hence, we introduce two normalization factors, z_p and z_q, and the normalized distributions are

$$\begin{cases} p^A(x)\big|_{\rm nor} = \dfrac{1}{\int_{x_{\rm min}}^{x_{\rm max}} p^A(x)dx}\, p^A(x) = z_p\, p^A(x), \\ q^d(x)\big|_{\rm nor} = \dfrac{1}{\int_{x_{\rm min}}^{x_{\rm max}} q^d(x)dx}\, q^d(x) = z_q\, q^d(x). \end{cases} \tag{8}$$

The KL divergence between the structure functions of nucleus A and the deuteron is calculated as follows:

$$D_{\rm KL}(p^A \| q^d) = \int_{x_{\rm min}}^{x_{\rm max}} p^A(x)\big|_{\rm nor} \ln \frac{p^A(x)\big|_{\rm nor}}{q^d(x)|_{\rm nor}}\, dx. \tag{9}$$

Here, $p^A(x)$ denotes the nuclear structure function constructed from the EPPS21 global analysis, and $q^d(x)$ represents the deuteron reference structure function built from the CT18A free PDFs. For the full-x region, more details are provided in Appendix A.

While the full-x KL divergence provides a useful global measure of the nuclear modification, the central goal of this work is to determine the shape of the structure function within the intermediate-x EMC region. We focus on this interval in what follows. In the EMC region, the ratio decreases monotonically from a maximum to a minimum. Within the EPPS21 set, this region spans $x \in [0.25, 0.65]$. We have also computed the KL divergence within this region using the same method described above, except that the integration limits in Eqs. (8) and (9) have been changed from $[10^{-6}, 0.99]$ to $[0.25, 0.65]$. More details about the resulting KL divergences for different nuclei are provided in Appendix A.

These results essentially quantify findings that are already known. More importantly, we are interested in whether the KL divergence can provide new insights into nucleon structure, especially in the EMC region. Prior to the discovery of the EMC effect, it was commonly believed that the ratio $(F_2^A(x)/A)/(F_2^d(x)/2)$ would be unity in the intermediate-x region, implying a corresponding KL divergence of zero. However, the EMC effect revealed that this ratio deviates from unity, showing a monotonic decrease in the approximate x-range from 0.25 to 0.65.

For a given nucleus A, if we fix the two endpoints at $x = 0.25$ and $x = 0.65$, a question arises: can we establish a criterion for determining the shape of the structure function within the EMC region? This is difficult because we are attempting to construct this function from insufficient data—neither perturbative QCD nor lattice QCD can be applied to this issue. Interestingly, the problem encountered here bears a striking resemblance to the famous brachistochrone problem proposed by Bernoulli in 1696 [59]. Both involve finding the extremum of a functional under fixed boundary conditions: the brachistochrone problem seeks the minimal time of descent, while our task requires establishing an extremum principle for a physical observable.

The physical observable we choose is the KL divergence utilized above.

$$D_{\rm KL}^{\rm EMC}(\hat{p}^A \| q^d) = \int_{0.25}^{0.65} \hat{p}^A(x)\big|_{\rm nor} \ln \frac{\hat{p}^A(x)\big|_{\rm nor}}{q^d(x)|_{\rm nor}}\, dx. \tag{10}$$

In the above equation, $\hat{p}^A(x)$ represents the structure function we aim to determine, and $q^d(x)$ denotes the deuteron reference distribution introduced above. We assume that, with the endpoints fixed, the actual structure function of the nucleus tends to minimize the KL divergence in Eq. (10), which we refer to as the "minimum relative entropy" hypothesis. It is important to emphasize that this hypothesis serves a role analogous to that of the shortest-time principle in the brachistochrone problem. With this hypothesis, the structure function can be computed and subsequently compared with the results of global fitting analyses. First, we adopt a polynomial parametrization for $\hat{p}^A(x)$.

$$\hat{p}^A_{\rm poly}(x) = \left(a_1 x^3 + b_1 x^2 + c_1 x + d_1\right) q^d(x). \tag{11}$$

Using the EPPS21 global fits, we can derive constraints at the endpoints, which determine two parameters in Eq. (11), while the remaining two are fixed by the minimum-relative-entropy hypothesis. It is worth noting that the two endpoint values at $x = 0.25$ and $x = 0.65$ are obtained from the EPPS21 global fits and thus encode direct experimental information about the nuclear modification at the boundaries of the EMC region. An alternative approach would be to employ momentum sum rules as theoretical constraints. However, sum rules are integral constraints over the full x-range; they do not directly fix the shape of distributions within the EMC sub-interval. Therefore, we did not adopt this method in the current work.

In Figure 1, we provide a two-dimensional visualization of the KL divergence as a function of the a_1 and b_1 parameters.[1)] The KL divergence forms a distribution in

1) From the perspective of artificial intelligence, the KL divergence here serves as a loss function defined over the parameter space. Figure 1 displays the corresponding loss landscape, where the minimum point (red dot) identifies the optimal solution under the imposed endpoint constraints.

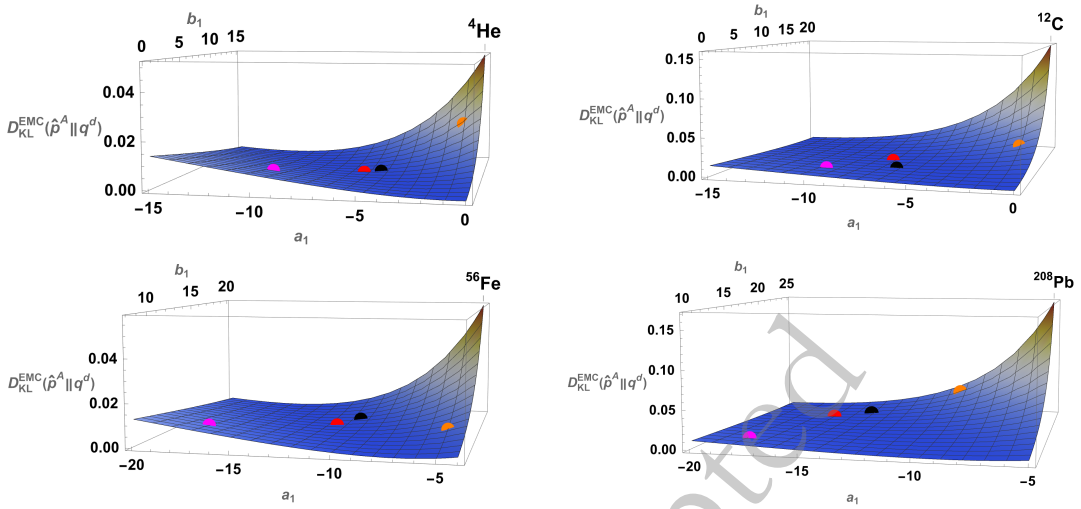

Fig. 1. (color online) The KL divergence is shown as a function of a_1 and b_1. The red dot indicates the position of the minimum KL divergence for ^{4}He, ^{12}C, ^{56}Fe, and ^{208}Pb at the momentum transfer $Q^2 = 10\,\mathrm{GeV}^2$. The orange and magenta dots mark two representative reference solutions, which will be used for comparison in Figure 2.

the parameter space that allows us to identify its minimum point. The position marked with a red dot indicates the corresponding a_1 and b_1 values that minimize the KL divergence. The black dot represents the result of the EPPS21 global analysis. These two points are found to be in close proximity within the parameter space. The structure functions corresponding to all four points will be presented in Figure 2.

We present the explicit results of the polynomial parametrization for ^{4}He, ^{12}C, ^{56}Fe, and ^{208}Pb.

$$\begin{aligned}
\hat{p}^{^4\mathrm{He}}_{\mathrm{poly}}(x) &= \left(-5.89\,x^3+7.39\,x^2-3.00\,x+1.38\right) q^d(x),\\
\hat{p}^{^{12}\mathrm{C}}_{\mathrm{poly}}(x) &= \left(-7.60\,x^3+9.53\,x^2-3.86\,x+1.48\right) q^d(x),\\
\hat{p}^{^{56}\mathrm{Fe}}_{\mathrm{poly}}(x) &= \left(-11.51\,x^3+14.43\,x^2-5.85\,x+1.72\right) q^d(x),\\
\hat{p}^{^{208}\mathrm{Pb}}_{\mathrm{poly}}(x) &= \left(-16.23\,x^3+20.32\,x^2-8.22\,x+1.99\right) q^d(x).
\end{aligned} \tag{12}$$

Appendix B lists the four parameters (a_1, b_1, c_1, and d_1) in Eq. (11).

Using the results in Eq. (12), we can plot the structure functions given by the minimum relative entropy hypothesis. Figure 2 shows a comparison between these structure functions and the global fitting results from the EPPS21 set. Additionally, for reference, we also plot two curves that yield larger KL divergences, corresponding to the orange and magenta dots in Figure 1, respectively. From Figure 2, it can be observed that the structure functions given by Eq. (12) are rather close to those obtained from the global analysis. This indicates that the minimum relative entropy hypothesis can yield reasonable nuclear structure functions, consistent with the results of the QCD global analysis.

In addition, we have examined the dependence of the results on the parametrization form. In Eq. (11), we adopted a polynomial form and expanded it to the cubic term x^3. We have also extended the expansion to the quartic term x^4, and the resulting $\hat{p}^A_{\mathrm{poly}}(x)$ remained identical to that obtained in the cubic case. Therefore, we do not show the corresponding results for the sake of brevity. Moreover, the widely used canonical parametrization form with exponential and power-law endpoint behaviour was also tested.

$$\hat{p}^A_{\mathrm{can}}(x) = \left(a_2 x^{b_2}(1-x)^{c_2} e^{d_2 x}\right) q^d(x). \tag{13}$$

Consistent with the previous method, these parameters can be determined using the minimum relative entropy hypothesis.

$$\begin{aligned}
\hat{p}^{^4\mathrm{He}}_{\mathrm{can}}(x) &= \left(0.20\,x^{-0.69}(1-x)^{1.39} e^{4.13x}\right) q^d(x),\\
\hat{p}^{^{12}\mathrm{C}}_{\mathrm{can}}(x) &= \left(0.13\,x^{-0.90}(1-x)^{1.81} e^{5.37x}\right) q^d(x),\\
\hat{p}^{^{56}\mathrm{Fe}}_{\mathrm{can}}(x) &= \left(0.039\,x^{-1.40}(1-x)^{2.84} e^{8.43x}\right) q^d(x),\\
\hat{p}^{^{208}\mathrm{Pb}}_{\mathrm{can}}(x) &= \left(0.008\,x^{-2.09}(1-x)^{4.25} e^{12.57x}\right) q^d(x).
\end{aligned} \tag{14}$$

Appendix B collects the values of the four parameters (a_2, b_2, c_2 and d_2) in Eq. (13).

We now summarize the key findings obtained so far. In Table 1, different KL divergences are compiled. The second column lists the KL divergence calculated using the results from the EPPS21 set, while the third and fourth columns present the minimum KL divergences calculated from Eq. (12) and Eq. (14), respectively. As can be seen, the obtained minimum KL divergences given by the polynomial and canonical parametrization forms

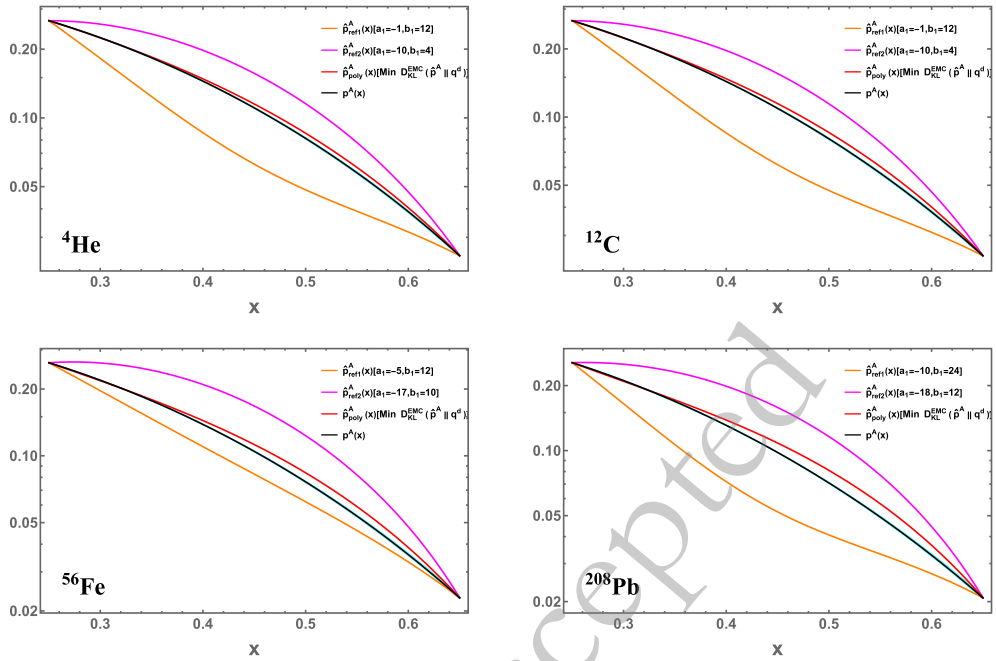

Fig. 2. (color online) Comparison of the structure functions $\hat{p}^A_{\rm poly}(x)$ obtained from the polynomial parameterization (red line), $p^A(x)$ from EPPS21 (black line), and the reference curves $\hat{p}^A_{\rm ref1}(x)$ (orange line) and $\hat{p}^A_{\rm ref2}(x)$ (magenta line).

Table 1. Comparisons of the KL divergence calculated from EPPS21 with the minimum KL divergences calculated using the polynomial and canonical parameterizations in the intermediate-x region [0.25,0.65] for different nuclei.

Nucleus	$D^{\rm EMC}_{\rm KL}(p^A\|\|q^d)$	$D^{\rm EMC}_{\rm KL}(\hat{p}^A_{\rm poly}\|\|q^d)$	$D^{\rm EMC}_{\rm KL}(\hat{p}^A_{\rm can}\|\|q^d)$
^{3}He	0.46×10^{-4}	1.3×10^{-5}	1.2×10^{-5}
^{4}He	2.32×10^{-4}	3.0×10^{-5}	2.9×10^{-5}
^{9}Be	4.75×10^{-4}	7.0×10^{-5}	6.9×10^{-5}
^{12}C	3.70×10^{-4}	5.0×10^{-5}	5.0×10^{-5}
^{56}Fe	8.17×10^{-4}	1.21×10^{-4}	1.21×10^{-4}
^{197}Au	16.19×10^{-4}	2.52×10^{-4}	2.58×10^{-4}
^{208}Pb	16.85×10^{-4}	2.63×10^{-4}	2.70×10^{-4}

show remarkable consistency with each other. This agreement becomes more visually discernible when the structure functions are displayed together. Figure 3 shows these two kinds of structure functions obtained from the polynomial and canonical parametrizations, as well as the global fitting results from the EPPS21 set. The differences between the structure functions obtained from these two parametrizations are visually indistinguishable.

It is instructive to examine how the parameters determined by the minimum relative entropy hypothesis depend on the nuclear species. In the polynomial parametrization, the leading cubic coefficient a_1 increases in magnitude monotonically from -5.89 (^{4}He) to -16.23 (^{208}Pb), reflecting the progressively stronger nuclear modification for heavier nuclei. Correspondingly, the minimum KL divergence $D^{\rm EMC}_{\rm KL}$ generally increases with the nuclear mass number A, consistent with the expectation that larger nuclei exhibit more pronounced deviations from the free-nucleon baseline. A notable exception is ^{9}Be, whose KL divergence exceeds that of ^{12}C. This non-monotonic behavior is consistent with findings in studies of nucleon short-range correlations and may be attributed to the unique cluster structure of beryllium.

These results demonstrate the robustness of the calculated minimum KL divergence across different parametrization forms. When the two endpoints in the intermediate-x region are fixed, both the value of the minimum KL divergence and the shape of the nuclear structure function are almost exclusively determined by the minimum relative entropy hypothesis. It should be emphasized that, although we adopt two commonly used parametrizations of the structure function, the values of their parameters are not determined by fitting. Instead, they are obtained by applying the minimum relative entropy hypothesis, which selects the parameters that minimize the relative entropy.

To quantify the perceived separation between the various structure functions and the global fit results provided by EPPS21 in Figures 2 and 3, we use the L^2 norm, which is defined as

$$N(\hat{p}^A_{\rm poly}) = \sqrt{\int_{0.25}^{0.65}\left(\hat{p}^A_{\rm poly}(x)-p^A(x)\right)^2 dx}, \qquad (15)$$

Here, $p^A(x)$ is the structure function from EPPS21. The results are listed in the second column of Table 2. It

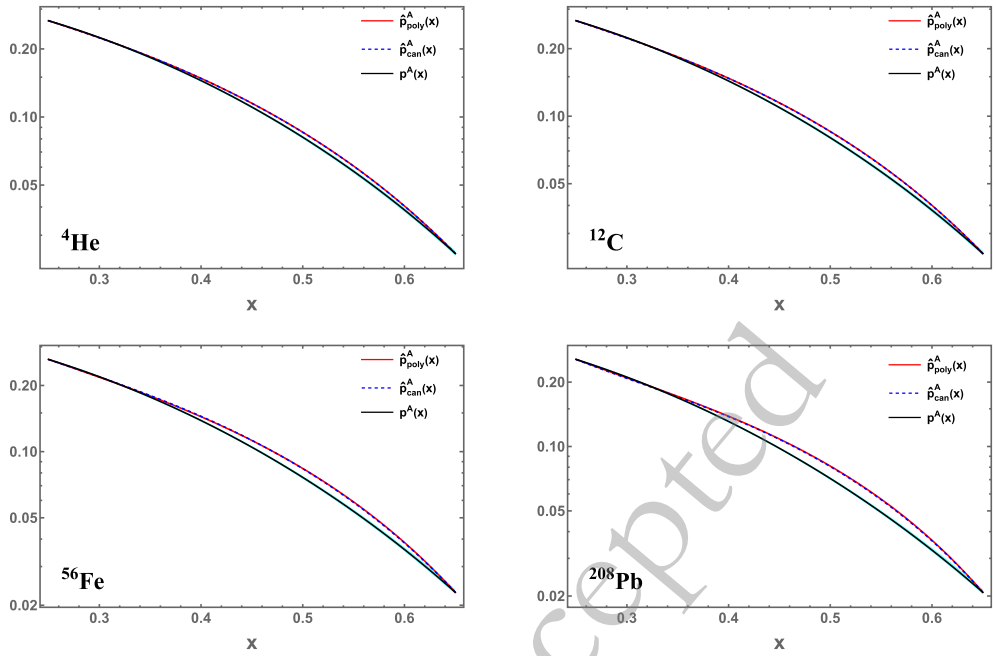

Fig. 3. (color online) Comparison of the structure functions $\hat{p}^A_{\rm poly}(x)$ obtained using the polynomial parameterization (red line), $\hat{p}^A_{\rm can}(x)$ obtained using the canonical parameterization (blue dashed line), and $p_A(x)$ from EPPS21 (black line).

Table 2. Norms of the structure functions with minimum KL divergences (second column) and of the reference structure functions (third and fourth columns).

Nucleus	$N(\hat{p}^A_{\rm poly})$ or $N(\hat{p}^A_{\rm can})$	$N(\hat{p}^A_{\rm ref1})$	$N(\hat{p}^A_{\rm ref2})$
^{3}He	6.61×10^{-4}	2.11×10^{-2}	2.33×10^{-2}
^{4}He	1.79×10^{-3}	2.50×10^{-2}	2.25×10^{-2}
^{9}Be	2.38×10^{-3}	4.07×10^{-2}	2.91×10^{-2}
^{12}C	2.20×10^{-3}	2.49×10^{-2}	2.26×10^{-2}
^{56}Fe	3.10×10^{-3}	1.22×10^{-2}	3.03×10^{-2}
^{197}Au	4.11×10^{-3}	1.34×10^{-2}	2.31×10^{-2}
^{208}Pb	4.14×10^{-3}	2.53×10^{-2}	2.89×10^{-2}

is evident that the norms calculated from $\hat{p}^A_{\rm poly}(x)$ are much smaller than those for the reference curves $\hat{p}^A_{\rm ref1}(x)$ and $\hat{p}^A_{\rm ref2}(x)$, indicating that the minimum relative entropy hypothesis could serve as a reliable criterion for constructing the quark structure functions of bound nucleons. Moreover, the two different parameterization forms (polynomial and canonical) yield nearly identical norms in Table 2.

These findings suggest that the discrepancy between the structure functions derived from the minimum relative entropy hypothesis and those obtained from global fits can be quantified by computing their L^2 norms. For the quark structure functions considered in this section, the minimum relative entropy hypothesis produces values close to those of the global fits, resulting in a small L^2 norm (on the order of 10^{-3} to 10^{-4}). In the following section, we adopt this norm-based comparison as a potential reference for evaluating the quality of global fits to gluon nPDFs.

V. DETERMINING GLUON NPDFS THROUGH KL DIVERGENCE

Nucleons are composed of quarks and gluons; therefore, investigating the distribution of gluons, the mediators of the strong interaction, within nuclei is of fundamental importance. However, our understanding of gluon nPDFs remains markedly poorer than that of quark nPDFs. This is reflected in the significant discrepancies among gluon nPDFs extracted by different global fitting groups, especially in the intermediate-x region. Whether gluons also exhibit the EMC effect is an open question under active investigation [60−71]. Our results in the previous section show that the minimum-relative-entropy hypothesis yields reasonable quark structure functions. In this section, we apply this hypothesis independently to gluon distributions.

We focus on gluon nPDFs in the intermediate-x region, where the results vary among different global fitting groups. Here, we adopt the results from two widely used global analyses, EPPS21[1)] [14] and nNNPDF3.0[2)] [15]. The KL divergence between the gluon nPDFs of nucleus A and deuteron is defined as

1) https://research.hip.fi/qcdtheory/nuclear-pdfs/epps21/

2) https://nnpdf.mi.infn.it/for-users/nnnpdf3-0/

$$D_{\mathrm{KL},g}^{\mathrm{EMC}}(p_g^A\|q_g^d)=\int_{x_{\min}}^{x_{\max}} p_g^A(x)\big|_{\mathrm{nor}}\ln\frac{p_g^A(x)\big|_{\mathrm{nor}}}{q_g^d(x)\big|_{\mathrm{nor}}}\,dx. \tag{16}$$

Here, $p_g^A(x)$ is taken as the true distribution and $q_g^d(x)$ as the reference distribution, with their values provided by global fitting groups. The limits of integration are set to $x_{\min}=0.25$, $x_{\max}=0.50$ for EPPS21 and to $x_{\min}=0.30$, $x_{\max}=0.55$ for nNNPDF3.0. These distributions require normalization analogous to that in Eq. (8). The calculated values of the normalization factors $z_{p,g}$ and $z_{q,g}$ for different nuclei are collected in Appendix A.

Following the minimum relative entropy hypothesis, we determine the shape of the gluon nPDFs $\hat{p}_g^A(x)$ that minimizes the relative entropy.

$$D_{\mathrm{KL},g}^{\mathrm{EMC}}(\hat{p}_g^A\|q_g^d)=\int_{x_{\min}}^{x_{\max}} \hat{p}_g^A(x)\big|_{\mathrm{nor}}\ln\frac{\hat{p}_g^A(x)\big|_{\mathrm{nor}}}{q_g^d(x)\big|_{\mathrm{nor}}}\,dx. \tag{17}$$

Similar to the quark case, the polynomial and canonical forms of the parameterizations are used to calculate $\hat{p}_g^A(x)$,

$$\hat{p}_{g,\mathrm{poly}}^A(x)=\left(a_1^g x^3+b_1^g x^2+c_1^g x+d_1^g\right)q_g^d(x), \tag{18}$$

$$\hat{p}_{g,\mathrm{can}}^A(x)=\left(a_2^g x^{b_2^g}(1-x)^{c_2^g}e^{d_2^g x}\right)q_g^d(x). \tag{19}$$

Following the same procedure outlined in the previous section for quarks, we now present the results directly. These are shown separately according to the global-fit dataset employed.

We begin with EPPS21: the explicit results for ^{4}He, ^{12}C, ^{56}Fe, and ^{208}Pb in the polynomial parametrization are as follows:

$$\begin{aligned}
\hat{p}_{g,\mathrm{poly}}^{^4\mathrm{He}}(x)&=\left(-29.62\,x^3+31.38\,x^2-10.89\,x+2.22\right)q_g^d(x),\\
\hat{p}_{g,\mathrm{poly}}^{^{12}\mathrm{C}}(x)&=\left(-36.95\,x^3+39.15\,x^2-13.58\,x+2.52\right)q_g^d(x),\\
\hat{p}_{g,\mathrm{poly}}^{^{56}\mathrm{Fe}}(x)&=\left(-50.10\,x^3+53.05\,x^2-18.40\,x+3.06\right)q_g^d(x),\\
\hat{p}_{g,\mathrm{poly}}^{^{208}\mathrm{Pb}}(x)&=\left(-64.57\,x^3+68.34\,x^2-23.69\,x+3.66\right)q_g^d(x),
\end{aligned} \tag{20}$$

and

$$\begin{aligned}
\hat{p}_{g,\mathrm{can}}^{^4\mathrm{He}}(x)&=\left(0.002\,x^{-2.56}(1-x)^{8.90}e^{21.19x}\right)q_g^d(x),\\
\hat{p}_{g,\mathrm{can}}^{^{12}\mathrm{C}}(x)&=\left(0.0004\,x^{-3.22}(1-x)^{11.20}e^{26.68x}\right)q_g^d(x),\\
\hat{p}_{g,\mathrm{can}}^{^{56}\mathrm{Fe}}(x)&=\left(0.003\,x^{-2.37}(1-x)^{9.83}e^{21.94x}\right)q_g^d(x),\\
\hat{p}_{g,\mathrm{can}}^{^{208}\mathrm{Pb}}(x)&=\left(0.002\,x^{-2.36}(1-x)^{10.92}e^{23.50x}\right)q_g^d(x),
\end{aligned} \tag{21}$$

for the canonical parametrization. Appendix B lists the calculated parameters (a_1^g, b_1^g, c_1^g and d_1^g) in Eq. (20) and (a_2^g, b_2^g, c_2^g and d_2^g) in Eq. (21) for different nuclei.

Using the results in Eqs. (20) and (21), we plot the gluon nPDFs obtained from the minimum relative entropy hypothesis in Figure 4. It can be observed that the shapes of the gluon nPDFs obtained from the two parameterizations are highly consistent, with differences between them barely discernible. Moreover, both results agree well with global fits to experimental data, falling within the uncertainty band of the EPPS21 results. It is worth noting that gluon nPDFs have relatively large uncertainties due to our currently limited knowledge of them. Therefore, the minimum relative entropy hypothesis may provide an even more useful complementary perspective for studying gluon nPDFs than for constraining quark structure functions.

Table 3 summarizes the different KL divergences. The second column lists the KL divergence calculated using the gluon nPDF results from the EPPS21 set, while the third and fourth columns correspond to the minimum KL divergences calculated according to Eq. (20) and Eq. (21), respectively. As observed for the quark structure function, the choice of parametrization does not significantly affect the values of the minimum KL divergence. Regarding the dependence of the determined parameters on the nuclear species, a similar systematic nuclear dependence is observed in the gluon sector: the polynomial coefficient a_1^g ranges from −29.62 (^{4}He) to −64.57 (^{208}Pb), indicating that gluon nuclear modifications also increase with A.

Similarly, the L^2 norm is used to quantify the differences between the parameterization results and the global fitting results. The norm values are collected in Table 4. It can be seen that the norms obtained from the two parameterizations differ only slightly. This supports the independence of the results with respect to the parameterization forms. The L^2 norms between the gluon nPDFs derived from the minimum relative entropy hypothesis and those obtained from the EPPS21 global fits range from 1.27×10^{-3} for ^{3}He to 1.05×10^{-2} for ^{208}Pb, providing a quantitative measure of the discrepancy between them.

We next turn to nNNPDF3.0. Applying this set of globally fitted gluon data in conjunction with the minimum relative entropy hypothesis, we obtain results for ^{4}He, ^{12}C, ^{56}Fe, and ^{208}Pb within the polynomial parametrization.

$$\begin{aligned}
\hat{p}_{g,\mathrm{poly}}^{^4\mathrm{He}}(x)&=\left(-8.97\,x^3+10.96\,x^2-4.41\,x+1.60\right)q_g^d(x),\\
\hat{p}_{g,\mathrm{poly}}^{^{12}\mathrm{C}}(x)&=\left(-47.08\,x^3+57.52\,x^2-23.11\,x+4.13\right)q_g^d(x),\\
\hat{p}_{g,\mathrm{poly}}^{^{56}\mathrm{Fe}}(x)&=\left(-216.67\,x^3+263.53\,x^2-105.39\,x+15.07\right)q_g^d(x),\\
\hat{p}_{g,\mathrm{poly}}^{^{208}\mathrm{Pb}}(x)&=\left(-389.23\,x^3+470.88\,x^2-187.19\,x+25.70\right)q_g^d(x).
\end{aligned} \tag{22}$$

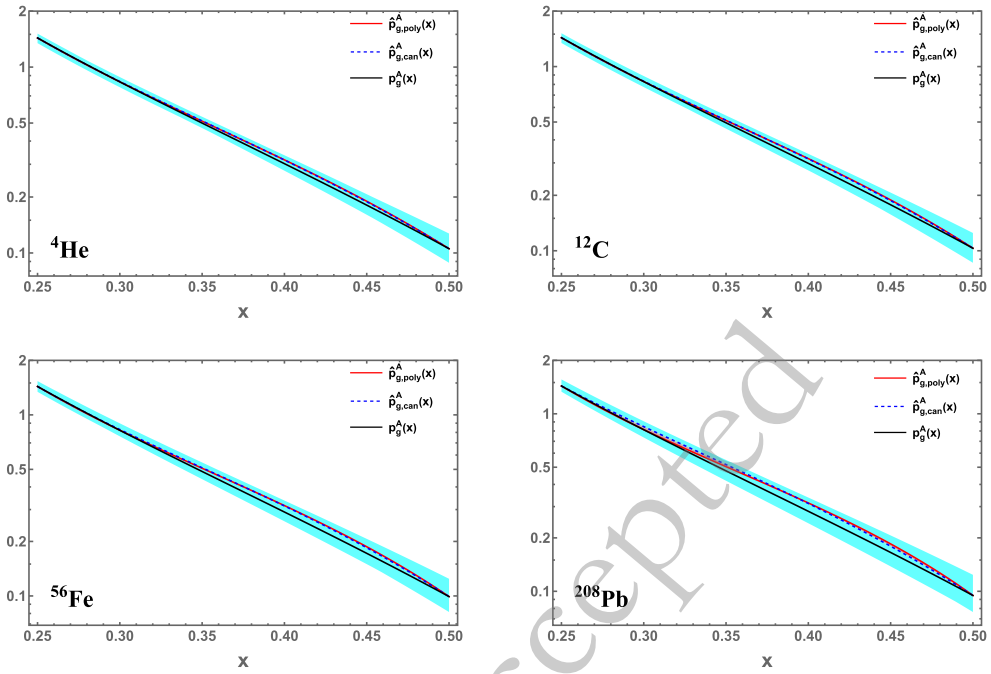

Fig. 4. (color online) Comparison of the gluon nPDFs: $\hat{p}^A_{g,\mathrm{poly}}(x)$ in the polynomial parametrization (red line), $\hat{p}^A_{g,\mathrm{can}}(x)$ in the canonical parametrization (blue dashed line), and $p^A_g(x)$ from EPPS21 (black line).

Table 3. The KL divergences from EPPS21 and those calculated using the polynomial and canonical parameterizations in the intermediate-x region [0.25,0.50] are shown. The four-momentum transfer is set to $Q^2 = 10\,\mathrm{GeV}^2$.

Nucleus	$D^{\mathrm{EMC}}_{\mathrm{KL},g}(p^A_g\|\|q^d_g)$	$D^{\mathrm{EMC}}_{\mathrm{KL},g}(\hat{p}^A_{g,\mathrm{poly}}\|\|q^d_g)$	$D^{\mathrm{EMC}}_{\mathrm{KL},g}(\hat{p}^A_{g,\mathrm{can}}\|\|q^d_g)$
^{3}He	1.54×10^{-5}	3.34×10^{-6}	3.44×10^{-6}
^{4}He	2.31×10^{-4}	4.66×10^{-5}	4.86×10^{-5}
^{9}Be	3.24×10^{-4}	6.51×10^{-5}	7.19×10^{-5}
^{12}C	3.65×10^{-4}	7.33×10^{-5}	7.70×10^{-5}
^{56}Fe	6.91×10^{-4}	1.37×10^{-4}	1.98×10^{-4}
^{197}Au	1.17×10^{-3}	2.28×10^{-4}	4.21×10^{-4}
^{208}Pb	1.19×10^{-3}	2.33×10^{-4}	3.95×10^{-4}

The corresponding canonical parametrization is

$$\begin{aligned}
\hat{p}^{^4\mathrm{He}}_{g,\mathrm{can}}(x) &= \left(0.0976\,x^{-1.03}(1-x)^{2.22}e^{6.33x}\right) q^d_g(x),\\
\hat{p}^{^{12}\mathrm{C}}_{g,\mathrm{can}}(x) &= \left(0.0014\,x^{-2.86}(1-x)^{7.16}e^{19.15x}\right) q^d_g(x),\\
\hat{p}^{^{56}\mathrm{Fe}}_{g,\mathrm{can}}(x) &= \left(0.0025\,x^{-2.20}(1-x)^{15.47}e^{30.52x}\right) q^d_g(x),\\
\hat{p}^{^{208}\mathrm{Pb}}_{g,\mathrm{can}}(x) &= \left(0.0002\,x^{-2.60}(1-x)^{31.26}e^{56.80x}\right) q^d_g(x). \qquad (23)
\end{aligned}$$

Appendix B compiles the calculated parameters (a^g_1, b^g_1, c^g_1, and d^g_1) in Eq. (22) and (a^g_2, b^g_2, c^g_2, and d^g_2) in Eq. (23).

The gluon nPDFs obtained from the minimum relative entropy hypothesis are shown in Fig. 5. Interestingly, these nPDFs begin to exhibit noticeable deviations from the nNNPDF3.0 results, with the discrepancy becoming particularly pronounced for ^{56}Fe and ^{208}Pb. The corresponding KL divergences are shown in Table 5. This discrepancy is more clearly illustrated by calculating the L^2 norms between the gluon nPDFs derived from the minimum relative entropy hypothesis and those obtained from the nNNPDF3.0 global fits. These values are presented in Table 6, where the norms are generally larger than those previously obtained with EPPS21. For example, the results for ^{56}Fe, ^{197}Au, and ^{208}Pb are approximately four times larger than their EPPS21 counterparts. In terms of central values, the EPPS21 gluon distributions are closer to the minimum relative entropy solutions obtained in the present analysis. However, because nNNPDF3.0 has significantly larger uncertainties and the endpoint uncertainties have not yet been considered, this comparison based on the minimum relative entropy hypothesis should be regarded as a potential reference rather than a benchmark.

Table 4. The norms of gluon nPDFs with minimal KL divergences.

Nucleus	$N(\hat{p}^A_{g,\mathrm{poly}})$	$N(\hat{p}^A_{g,\mathrm{can}})$
^{3}He	1.27×10^{-3}	1.25×10^{-3}
^{4}He	4.70×10^{-3}	4.58×10^{-3}
^{9}Be	5.54×10^{-3}	5.45×10^{-3}
^{12}C	5.87×10^{-3}	5.70×10^{-3}
^{56}Fe	8.02×10^{-3}	9.05×10^{-3}
^{197}Au	1.03×10^{-2}	1.15×10^{-2}
^{208}Pb	1.05×10^{-2}	1.28×10^{-2}

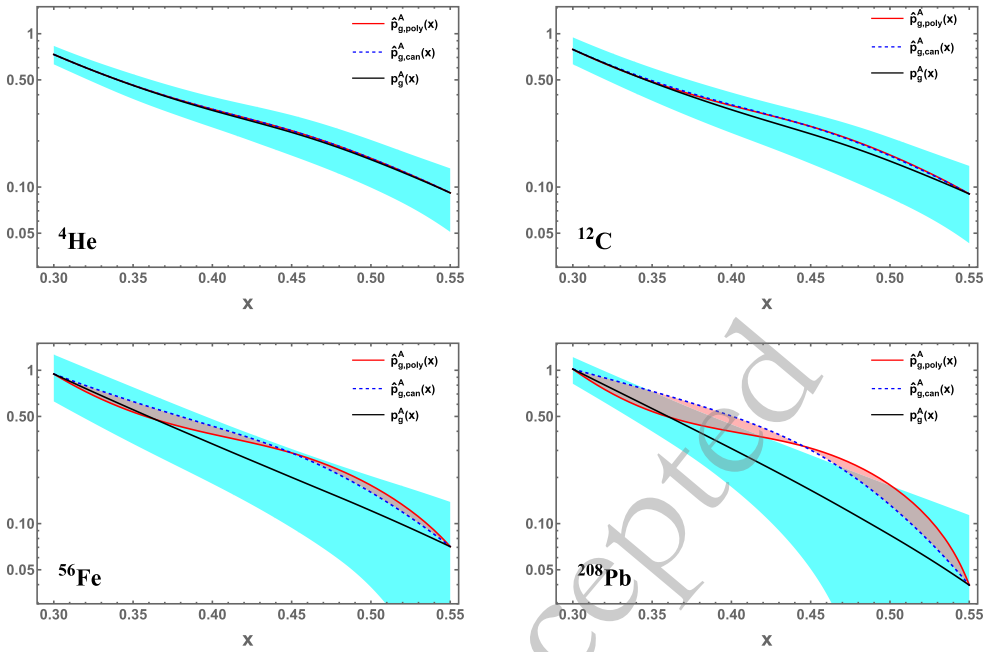

Fig. 5. (color online) The same as Figure 4, but for nNNPDF3.0.

Table 5. Same as Table 3, but for the nNNPDF3.0 gluon nPDFs in the intermediate-x region $[0.30, 0.55]$.

Nucleus	$D^{\rm EMC}_{{\rm KL},g}(p^A_g\|\|q^d_g)$	$D^{\rm EMC}_{{\rm KL},g}(\hat{p}^A_{g,{\rm poly}}\|\|q^d_g)$	$D^{\rm EMC}_{{\rm KL},g}(\hat{p}^A_{g,{\rm can}}\|\|q^d_g)$
^{4}He	4.55×10^{-5}	4.27×10^{-6}	4.30×10^{-6}
^{9}Be	5.23×10^{-4}	5.34×10^{-5}	6.93×10^{-5}
^{12}C	1.02×10^{-3}	1.07×10^{-4}	1.50×10^{-4}
^{56}Fe	1.45×10^{-2}	1.93×10^{-3}	5.30×10^{-3}
^{197}Au	3.69×10^{-2}	5.49×10^{-3}	1.66×10^{-2}
^{208}Pb	4.38×10^{-2}	6.53×10^{-3}	2.21×10^{-2}

Table 6. The same as Table 4, but for the nNNPDF3.0 gluon nPDFs.

Nucleus	$N(\hat{p}^A_{g,{\rm poly}})$	$N(\hat{p}^A_{g,{\rm can}})$
^{4}He	1.69×10^{-3}	1.85×10^{-3}
^{9}Be	5.97×10^{-3}	6.12×10^{-3}
^{12}C	8.25×10^{-3}	8.78×10^{-3}
^{56}Fe	2.72×10^{-2}	3.52×10^{-2}
^{197}Au	4.11×10^{-2}	5.26×10^{-2}
^{208}Pb	4.43×10^{-2}	6.59×10^{-2}

The results of this work are intriguing and warrant further investigation to uncover the profound physical connections between PDFs and nPDFs within the framework of quantum information theory. The behavior of nonperturbative QCD is highly complex. In contrast to conventional approaches, the concept of entropy offers a promising avenue for elucidating the fundamental symmetries and underlying dynamics of QCD that are otherwise hidden.

In addition, it is worth noting that the present analysis is restricted to the EMC region, where the nuclear modification exhibits smooth and monotonic behavior that is well suited to the minimum relative entropy hypothesis employed here. Extending the methodology to the full kinematic range would require addressing the qualitatively different behaviors in the shadowing, antishadowing, and Fermi-motion regions. Such an extension necessitates additional physical inputs—for instance, multiple sets of boundary conditions and constraints from parton momentum sum rules—and is left for future investigation.

VI. CONCLUDING REMARKS

In this work, beyond conventional observables, we have introduced the KL divergence, a well-known quantity in quantum information theory, as a measure for probing the parton structure of nucleons bound in nuclei. In the quark sector, the resulting structure functions in the EMC region are broadly consistent with current global analyses. In the gluon sector, the minimum relative entropy hypothesis provides an information-theoretic perspective for comparing different global analyses. The present results indicate that, at the level of central values, the EPPS21 gluon distributions are closer to the minimum relative entropy solutions obtained here, while a clearer assessment of nNNPDF3.0 requires further study. These observations suggest that the KL-divergence approach may serve as a useful complementary tool in future studies of nPDFs.

In particle physics, determining nonperturbative inputs beyond global fitting is not only complementary but also necessary for a deeper understanding of hadron structure. The introduction of the KL divergence and the minimum relative entropy hypothesis offers a new perspective on longstanding problems. The present framework may help further explore the details of nuclear structure functions and parton distributions. Admittedly, the results presented here should still be regarded as indicative rather than definitive, and we hope that this work will stimulate further studies of information-theoretic approaches to nucleon structure.

ACKNOWLEDGEMENTS

The authors would like to thank Prof. Wei Wang and Shuai Zhao for fruitful and inspiring discussions.

APPENDIX A: DETAILS OF THE KL-DIVERGENCE CALCULATIONS

Here, we compute the KL divergence using Eqs. (8) and (9). The corresponding integration limits are $[10^{-6},0.99]$ and $[0.25,0.65]$, respectively. The resulting KL divergences are denoted by $D_{\rm KL}^{\rm full}(p^A\|q^d)$ and $D_{\rm KL}^{\rm EMC}(p^A\|q^d)$. Table A1 presents the calculated KL divergences for different nuclei.

We use the EPPS21 nPDF set together with the CT18A free-PDF set. For the full-x region $[10^{-6},0.99]$ and the intermediate-x region $[0.25,0.65]$, we take $F_2^A(x,Q^2)/A$ as $p^A(x)$ in Eq. (6) and $F_2^d(x,Q^2)/2$ as $q^d(x)$. Qualitatively, as A increases, nuclear modification becomes more apparent, leading to an increase in the KL divergence —a trend that is consistent with the results shown in Table A1. However, it is worth noting that the value for ^{12}C is lower than that for ^{9}Be, a pattern consistent with findings from studies of nucleon short-range correlations, which show a non-monotonic dependence on A for ^{12}C and ^{9}Be [72]. This may arise from the unique nature of beryllium, whose density is similar to that of helium, yet whose EMC effect closely resembles that of denser nuclei because of its pronounced cluster structure.

The values of the normalization factors z_p and z_q defined in Eq. (8) are listed in Table A2.

Table A3 presents the normalization factors used to calculate the gluon KL divergence.

Table A4 presents the normalization factors used to

Table A1. The KL divergences for different nuclei are evaluated in the full-x region $[10^{-6},0.99]$ and the intermediate-x region $[0.25,0.65]$. The four-momentum transfer is chosen as $Q^2=10\,\mathrm{GeV}^2$.

Nucleus	$D_{\rm KL}^{\rm full}(p^A\|q^d)$	$D_{\rm KL}^{\rm EMC}(p^A\|q^d)$
^{3}He	1.33×10^{-3}	0.46×10^{-4}
^{4}He	5.00×10^{-3}	2.32×10^{-4}
^{9}Be	5.22×10^{-3}	4.75×10^{-4}
^{12}C	5.42×10^{-3}	3.70×10^{-4}
^{56}Fe	6.38×10^{-3}	8.17×10^{-4}
^{197}Au	7.93×10^{-3}	16.19×10^{-4}
^{208}Pb	8.03×10^{-3}	16.85×10^{-4}

Table A2. The normalization factors z_p and z_q are shown for different nuclei in the full-x region $[10^{-6},0.99]$ and the intermediate-x region $[0.25,0.65]$. The four-momentum transfer is chosen as $Q^2=10\,\mathrm{GeV}^2$.

Nucleus	$z_p^{\rm full}$	$z_p^{\rm EMC}$
^{2}D(z_q)	7.06	19.61
^{3}He	6.70	18.16
^{4}He	7.12	20.32
^{9}Be	7.26	21.05
^{12}C	7.14	20.48
^{56}Fe	7.27	21.16
^{197}Au	7.48	22.20
^{208}Pb	7.50	22.29

Table A3. Normalization factors $z_{p,g}^{\rm EMC}$ and $z_{q,g}^{\rm EMC}$ used in the calculation of the EPPS21 gluon KL divergence in the intermediate-x region $[0.25,0.5]$.

Nucleus	$z_{p,g}^{\rm EMC}$
^{2}D($z_{q,g}$)	7.67
^{3}He	7.74
^{4}He	7.93
^{9}Be	7.97
^{12}C	7.98
^{56}Fe	8.09
^{197}Au	8.20
^{208}Pb	8.21

Table A4. Same as Table A3, but for the nNNPDF3.0 gluon nPDFs in the intermediate-x region $[0.3,0.55]$.

Nucleus	$z_{p,g}^{\rm EMC}$
^{2}D($z_{q,g}$)	13.03
^{4}He	12.99
^{9}Be	12.79
^{12}C	12.65
^{56}Fe	11.94
^{197}Au	12.32
^{208}Pb	12.48

Table B1. For the quark case, the parameters determined using the polynomial form in Eq. (11) and the canonical form in Eq. (13) are given for different nuclei. The integration interval is $x \in [0.25, 0.65]$.

Nucleus	a_1	b_1	c_1	d_1	a_2	b_2	c_2	d_2
^{3}He	4.29	−5.39	2.19	0.79	2.99	0.45	−0.90	−2.68
^{4}He	−5.89	7.39	−3.00	1.38	0.20	−0.69	1.39	4.13
^{9}Be	−8.75	10.97	−4.45	1.54	0.08	−1.06	2.15	6.37
^{12}C	−7.60	9.53	−3.86	1.48	0.13	−0.90	1.81	5.37
^{56}Fe	−11.51	14.43	−5.85	1.72	0.039	−1.40	2.84	8.43
^{197}Au	−15.94	19.97	−8.08	1.98	0.009	−2.04	4.16	12.30
^{208}Pb	−16.23	20.32	−8.22	1.99	0.008	−2.09	4.25	12.57

calculate the KL divergence for the nNNPDF3.0 gluon.

APPENDIX B: COLLECTION OF DETERMINED PARAMETERS

In this appendix, we collect the parameters determined for the polynomial and canonical parameterizations. For the quark case, we provide the four parameters (a_1, b_1, c_1 and d_1) in Eq. (11) and the four parameters (a_2, b_2, c_2 and d_2) in Eq. (13), which are determined by imposing endpoint constraints and minimizing the KL divergences in Eq. (10) for different nuclei.

For the gluon case, after applying the EPPS21 global fit for gluon nPDFs and the minimum relative entropy hypothesis, we present the four parameters (a_1^g, b_1^g, c_1^g, and d_1^g) in Eq. (20) and the four parameters (a_2^g, b_2^g, c_2^g, and d_2^g) in Eq. (21), which are determined by endpoint constraints and by minimizing the KL divergences in Eq. (17) for different nuclei.

Table B2. For the gluon case, the parameters are determined in polynomial form in Eq. (18) and in canonical form in Eq. (19) for different nuclei using the EPPS21 global fits. The integration interval is $x \in [0.25, 0.50]$.

Nucleus	a_1^g	b_1^g	c_1^g	d_1^g	a_2^g	b_2^g	c_2^g	d_2^g
^{3}He	−8.09	8.57	−2.98	1.33	0.20	−0.65	2.29	5.43
^{4}He	−29.62	31.38	−10.89	2.22	0.002	−2.56	8.90	21.19
^{9}Be	−34.85	36.92	−12.81	2.44	0.002	−2.49	9.06	21.22
^{12}C	−36.95	39.15	−13.58	2.52	0.0004	−3.22	11.20	26.68
^{56}Fe	−50.10	53.05	−18.40	3.06	0.003	−2.37	9.83	21.94
^{197}Au	−60.90	67.63	−23.44	3.63	0.006	−2.00	9.40	20.05
^{208}Pb	−64.57	68.34	−23.69	3.66	0.002	−2.36	10.92	23.50

Table B3. Same as Table B2, but for the nNNPDF3.0 gluon nPDFs in the intermediate-x region, $[0.3, 0.55]$.

Nucleus	a_1^g	b_1^g	c_1^g	d_1^g	a_2^g	b_2^g	c_2^g	d_2^g
^{4}He	−8.97	10.96	−4.41	1.60	0.0976	−1.03	2.22	6.33
^{9}Be	−32.70	39.96	−16.06	3.17	0.0060	−2.24	5.44	14.74
^{12}C	−47.08	57.52	−23.11	4.13	0.0014	−2.86	7.16	19.15
^{56}Fe	−216.67	263.53	−105.39	15.07	0.0025	−2.20	15.47	30.52
^{197}Au	−359.78	435.71	−173.42	23.93	$1.58 * 10^{-6}$	−4.96	30.91	62.49
^{208}Pb	−389.23	470.88	−187.19	25.70	0.0002	−2.60	31.26	56.80

For the gluon case, after applying the nNNPDF3.0 global fit to gluon nPDFs and the minimum relative entropy hypothesis, we present the four parameters (a_1^g, b_1^g, c_1^g and d_1^g) in Eq. (22) and the four parameters (a_2^g, b_2^g, c_2^g and d_2^g) in Eq. (23), which are determined by endpoint constraints and by minimizing the KL divergences in Eq. (17) for different nuclei.

References

[1] T. J. Hou, J. Gao, T. J. Hobbs, K. Xie, S. Dulat, M. Guzzi, J. Huston, P. Nadolsky, J. Pumplin and C. Schmidt, *et al.*, Phys. Rev. D **103**(1), 014013 (2021), arXiv: 1912.10053[hep-ph]

[2] S. Bailey, T. Cridge, L. A. Harland-Lang, A. D. Martin and R. S. Thorne, Eur. Phys. J. C **81**(4), 341 (2021), arXiv: 2012.04684[hep-ph]

[3] H. L. Lai, M. Guzzi, J. Huston, Z. Li, P. M. Nadolsky, J. Pumplin and C. P. Yuan, Phys. Rev. D **82**, 074024 (2010), arXiv: 1007.2241[hep-ph]

[4] A. D. Martin, W. J. Stirling, R. S. Thorne and G. Watt, Eur. Phys. J. C **63**, 189 (2009), arXiv: 0901.0002[hep-ph]

[5] S. Alekhin, J. Blumlein and S. Moch, Phys. Rev. D **86**, 054009 (2012), arXiv: 1202.2281[hep-ph]

[6] V. Barone, A. Drago and B. Q. Ma, Phys. Rev. C **62**, 062201 (2000), arXiv: hep-ph/0011334[hep-ph]

[7] J. J. Aubert *et al.* [European Muon], Phys. Lett. B **123**, 275 (1983)

[8] D. Allasia *et al.* [New Muon (NMC)], Phys. Lett. B **249**, 366 (1990)

[9] J. Gomez, R. G. Arnold, P. E. Bosted, C. C. Chang, A. T. Katramatou, G. G. Petratos, A. A. Rahbar, S. E. Rock, A. F. Sill and Z. M. Szalata, *et al.*, Phys. Rev. D **49**, 4348 (1994)

[10] J. Seely, A. Daniel, D. Gaskell, J. Arrington, N. Fomin, P. Solvignon, R. Asaturyan, F. Benmokhtar, W. Boeglin and B. Boillat, *et al.*, Phys. Rev. Lett. **103**, 202301 (2009), arXiv: 0904.4448[nucl-ex]

[11] W. Detmold *et al.* [NPLQCD], Phys. Rev. Lett. **126**(20), 202001 (2021), arXiv: 2009.05522[hep-lat]

[12] S. Amarasinghe, R. Baghdadi, Z. Davoudi, W. Detmold, M. Illa, A. Parreno, A. V. Pochinsky, P. E. Shanahan and M. L. Wagman, Phys. Rev. D **107**, no.9, 094508 (2023)[erratum: Phys. Rev. D **110**, no.11, 119904 (2024)] doi: 10.1103/PhysRevD.107.094508 [arXiv: 2108.10835[hep-lat]].

[13] C. Chen *et al.* [CLQCD and Lattice Parton], Phys. Rev. D **111**(7), 074506 (2025), arXiv: 2408.12819[hep-lat]

[14] K. J. Eskola, P. Paakkinen, H. Paukkunen and C. A. Salgado, Eur. Phys. J. C **82**(5), 413 (2022), arXiv: 2112.12462[hep-ph]

[15] R. Abdul Khalek, R. Gauld, T. Giani, E. R. Nocera, T. R. Rabemananjara and J. Rojo, Eur. Phys. J. C **82**(6), 507 (2022), arXiv: 2201.12363[hep-ph]

[16] P. Duwentäster, T. Ježo, M. Klasen, K. Kovařík, A. Kusina, K. F. Muzakka, F. I. Olness, R. Ruiz, I. Schienbein and J. Y. Yu, Phys. Rev. D **105**(11), 114043 (2022), arXiv: 2204.09982[hep-ph]

[17] I. Helenius, M. Walt and W. Vogelsang, Phys. Rev. D **105**(9), 094031 (2022), arXiv: 2112.11904[hep-ph]

[18] A. Galindo and M. A. Martin-Delgado, Rev. Mod. Phys. **74**, 347 (2002), arXiv: quant-ph/0112105[quant-ph]

[19] T. M. Cover and J. A. Thomas, *Elements of Information Theroy* (2nd ed.). Wiley-Interscience.

[20] R. Wang and X. Chen, Phys. Rev. D **91**, 054026 (2015), arXiv: 1410.3598[hep-ph]

[21] D. E. Kharzeev and E. M. Levin, Phys. Rev. D **95**(11), 114008 (2017), arXiv: 1702.03489[hep-ph]

[22] S. R. Beane, D. B. Kaplan, N. Klco and M. J. Savage, Phys. Rev. Lett. **122**(10), 102001 (2019), arXiv: 1812.03138[nucl-th]

[23] E. Gotsman and E. Levin, Phys. Rev. D **102**(7), 074008 (2020), arXiv: 2006.11793[hep-ph]

[24] S. Fedida and A. Serafini, Phys. Rev. D **107**(11), 116007 (2023), arXiv: 2209.01405[quant-ph]

[25] M. Hentschinski, K. Kutak and R. Straka, Eur. Phys. J. C **82**(12), 1147 (2022), arXiv: 2207.09430[hep-ph]

[26] Q. Liu, I. Low and T. Mehen, Phys. Rev. C **107**(2), 025204 (2023), arXiv: 2210.12085[quant-ph]

[27] C. Han, G. Xie, R. Wang and X. Chen, Eur. Phys. J. C **81**(4), 302 (2021), arXiv: 2010.14284[hep-ph]

[28] C. W. Ma and Y. G. Ma, Prog. Part. Nucl. Phys. **99**, 120 (2018), arXiv: 1801.02192[nucl-th]

[29] Y. Hagiwara, Y. Hatta, B. W. Xiao and F. Yuan, Phys. Rev. D **97**(9), 094029 (2018), arXiv: 1801.00087[hep-ph]

[30] V. Vedral, Rev. Mod. Phys. **74**, 197 (2002), arXiv: quant-ph/0102094[quant-ph]

[31] S. i. Nam, [arXiv: 2506.10672[hep-ph]].

[32] G. A. Miller, Phys. Rev. C **108**(3), L031002 (2023), arXiv: 2306.03239[nucl-th]

[33] S. Zhang, X. Wang, T. Lin and L. Chang, Chin. Phys. C **48**(3), 033106 (2024), arXiv: 2309.01417[hep-ph]

[34] H. Bloss, B. Kriesten and T. J. Hobbs, [arXiv: 2503.15603[hep-ph]].

[35] T. R. Hu, S. Chen, K. Sone, F. K. Guo, T. Hyodo and I. Low, [arXiv: 2507.22694[hep-ph]].

[36] X. Wang, Y. Shi, N. Wang, J. Yun, J. Li, Y. Jia, S. Liu, Z. Lu, J. Zou and Y. Li, [arXiv: 2504.18795[quant-ph]].

[37] S. J. Lin, M. J. Liu, D. Y. Shao and S. Y. Wei, [arXiv: 2507.15387[hep-ph]].

[38] S. Kullback and R. A. Leibler, The Annals of Mathematical Statistics **22**(1), 79 (1951)

[39] A. Wehrl, Rev. Mod. Phys. **50**, 221 (1978)

[40] G. Benito-Calviño, J. García-Olivares and F. J. Llanes-Estrada, Nucl. Phys. A **1036**, 122670 (2023), arXiv: 2209.13225[hep-ph]

[41] Q. H. Cao and D. Ueda, Phys. Rev. D **108**(2), 025011 (2023), arXiv: 2201.00931[hep-th]

[42] Q. H. Cao, N. Kan and D. Ueda, JHEP **07**, 111 (2023), arXiv: 2211.08065[hep-th]

[43] C. G. Callan, Jr. and D. J. Gross, Phys. Rev. Lett. **22**, 156 (1969)

[44] S. Navas *et al*. [Particle Data Group], Phys. Rev. D **110**(3), 030001 (2024)

[45] J. Collins, *Foundations of perturbative QCD*. Cambridge University Press.

[46] O. Hen, G. A. Miller, E. Piasetzky and L. B. Weinstein, Rev. Mod. Phys. **89**(4), 045002 (2017), arXiv: 1611.09748[nucl-ex]

[47] A. Radyushkin and S. Zhao, JHEP **02**, 163 (2022), arXiv: 2201.02181[hep-ph]

[48] J. H. Zhang, X. Ji, A. Schäfer, W. Wang and S. Zhao, Phys. Rev. Lett. **122**(14), 142001 (2019), arXiv: 1808.10824[hep-ph]

[49] L. Frankfurt, V. Guzey and M. Strikman, Phys. Rept. **512**, 255 (2012), arXiv: 1106.2091[hep-ph]

[50] L. B. Chen, W. Wang and R. Zhu, Phys. Rev. Lett. **126**(7), 072002 (2021), arXiv: 2006.14825[hep-ph]

[51] K. b. Chen, S. y. Wei and Z. t. Liang, Front. Phys. (Beijing) **10**(6), 101204 (2015), arXiv: 1506.07302[hep-ph]

[52] S. y. Wei, Y. k. Song, K. b. Chen and Z. t. Liang, Phys. Rev. D **95**(7), 074017 (2017), arXiv: 1611.08688[hep-ph]

[53] https://research.hip.fi/qcdtheory/nuclear-pdfs/epps21/

[54] P. Amaudruz *et al*. [New Muon], Nucl. Phys. B **441**, 3 (1995), arXiv: hep-ph/9503291[hep-ph]

[55] M. Arneodo *et al*. [New Muon], Nucl. Phys. B **441**, 12 (1995), arXiv: hep-ex/9504002[hep-ex]

[56] M. Arneodo *et al*. [New Muon], Nucl. Phys. B **481**, 3 (1996)

[57] M. Arneodo *et al*. [New Muon], Nucl. Phys. B **481**, 23 (1996)

[58] J. Ashman *et al*. [European Muon], Z. Phys. C **57**, 211 (1993)

[59] Johann Bernoulli, *Problema novum ad cujus solutionem Mathematici invitantur*. Acta Eruditorum, 18 : 269.

[60] J. W. Chen, W. Detmold, J. E. Lynn and A. Schwenk, Phys. Rev. Lett. **119**(26), 262502 (2017), arXiv: 1607.03065[hep-ph]

[61] R. Wang, X. Chen and Q. Fu, Nucl. Phys. B **920**, 1 (2017), arXiv: 1611.03670[hep-ph]

[62] J. Xu and F. Yuan, Phys. Lett. B **801**, 135187 (2020), arXiv: 1908.10413[hep-ph]

[63] Y. Hatta, M. Strikman, J. Xu and F. Yuan, Phys. Lett. B **803**, 135321 (2020), arXiv: 1911.11706[hep-ph]

[64] X. G. Wang, A. W. Thomas and W. Melnitchouk, Phys. Rev. Lett. **125**, 262002 (2020), arXiv: 2004.03789[hep-ph]

[65] X. G. Wang, W. Bentz, I. C. Cloët and A. W. Thomas, J. Phys. G **49**(3), 03LT01 (2022), arXiv: 2109.03591[hep-ph]

[66] W. Wang, J. Xu, X. H. Yang, Y. T. Zhang and S. Zhao, [arXiv: 2409.14367[hep-ph]].

[67] X. H. Yang, F. Huang and J. Xu, Phys. Rev. D **108**(5), 053005 (2023), arXiv: 2305.11538[hep-ph]

[68] R. Wang, N. N. Ma and T. F. Wang, Chin. Phys. C **47**(4), 044103 (2023), arXiv: 2207.10980[nucl-th]

[69] F. Huang, J. Xu and X. H. Yang, Phys. Rev. D **104**(3), 033002 (2021), arXiv: 2103.07873[hep-ph]

[70] W. Wang, J. Xu, X. H. Yang and S. Zhao, Eur. Phys. J. A **61**(5), 112 (2025), arXiv: 2401.16662[hep-ph]

[71] S. M. Hu, Y. S. Luan and J. Xu, Chin. Phys. C **47**(9), 093102 (2023), arXiv: 2112.14549[hep-ph]

[72] B. Schmookler *et al*. [CLAS], Nature **566**(7744), 354 (2019), arXiv: 2004.12065[nucl-ex]

[73] R. Francener, V. P. Goncalves and D. R. Gratieri, JHEP **01**, 149 (2026), arXiv: 2509.00144[hep-ph]

[74] S. M. Hu, W. Wang, J. Xu, X. H. Yang and S. Zhao, [arXiv: 2601.11867[hep-ph]].